Chemistry Africa
https://doi.org/10.1007/s42250-025-01186-3

ORIGINAL ARTICLE

Preparation and Application of Cow Dung Biochar Adsorbent in Removal of Pesticide Residues and Polycyclic Aromatic Hydrocarbons (PAHs) From Water

Bakari Chaka[1] · Aloys M. Osano[1] · Omwoyo N. Wesley[1] · Patricia B. C. Forbes[2]

Received: 9 September 2024 / Accepted: 2 January 2025

Abstract
This study aimed at preparing and assessing the potential of cow dung biochar (CDB) in adsorption of selected pesticides (tebuconazole, λ-cyhalothrin and α-cypermethrin) and polycyclic aromatic hydrocarbons (PAHs) (naphthalene, phenanthrene and anthracene) from water. CDB was prepared by low temperature pyrolysis (300–350 ℃) and characterized for surface morphology, composition, crystallinity, phases and thermal properties before assessing its adsorption efficacy at different conditions, isotherm models and regeneration capacity for the target pesticides and PAHs. The morphologies of the samples indicated an amorphous structurewith –OH groups. The composite char had four phases of amorphous, transition, composite and turbostratic char phase while depicting high thermally stability. The adsorption capacities ranged between 78 and 91%. The optimal adsorption conditions were 20 ℃ at a pH range of 4.0–8.0 for 30 min. Temkins adsorption was the most favored model. Chemisorption was exhibited for all sorbates except λ-cyhalothrin while following both pseudo-first order and Akrami-Erovich models. The adsorption processes were spontaneous under room temperature conditions. The adsorbents had an adsorption capacity of 63–80% for the third adsorption cycle indicating they would be regenerated successfully. As a matter of fact, the prepared CBD showed potential for removal of the chemical pollutants' removal.

Keywords Pesticides · PAHs · Cow dung biochar · Adsorption

1 Introduction

Access to clean water is a basic human and animal requirement. Water safety is determined based on World Health Organization (WHO) Clean Water Guidelines [1]. The traditional metrics for clean water have been based on physicochemical properties and waterborne microbes. However, there are emerging chemical pollutants (ECPs) from both point and diffuse sources, including Polycyclic Aromatic Hydrocarbons (PAHs) and pesticides [2]. The pollutants originate from agricultural activities, industrial wastewater and fossil fuel combustion and end up in water bodies consequently affecting the environment. These pollutants (specifically pesticides and low molecular-weight PAHs) are quite soluble in water with half-lives that are long enough to cause significant effects to the environment [3]. Some ECPs are carcinogenic and mutagenic to both humans and livestock [4].

A wide range of PAHs have been detected in water and sediments [5] and are relatively soluble in water, with their lipophilicity decreasing with molecular weight [4]. These compounds are made up of carbon and hydrogen in two or more fused aromatic rings. The molecular weight of PAHs is quite significant as it affects their lipophilicity as well as their atmospheric mobility and volatility [6–8]. In addition, PAHs in water associate freely with dissolved organic matter via binding and adsorption [9] which may lead to aquatic toxicity. Bio-availability of PAHs in water and

✉ Bakari Chaka
bakarichaka@mmarau.ac.ke

Aloys M. Osano
aloysosano@mmarau.ac.ke

Omwoyo N. Wesley
wesleyomwoyo@mmarau.ac.ke

Patricia B. C. Forbes
patricia.forbes@up.ac.za

[1] Department of Mathematics and Physical Sciences, Maasai Mara University, P.O Box 861-20500, Narok, Kenya

[2] Department of Chemistry, Faculty of Agriculture and Natural Sciences, University of Pretoria, Pretoria 0002, South Africa

Published online: 16 January 2025

consequent exposure of animals through food and water has thus become a global ecological challenge [10]. In this regard, PAHs pose serious health challenges with several of them being classified as carcinogenic, mutagenic and teratogenic [6, 7].

It is worth mentioning that pesticides have unique mobility in soil increasing their probability of ultimately leaching and seeping into water bodies [11]. Several pesticides are soluble or have solubilizers to ensure they can be easily conveyed by water during spraying as well as absorbed by plants or the target organisms. Most pesticides can stay in water for long periods; with half-lives of up to 50 years [12]. Lipophilic pesticides such as some of the organochlorines can also be absorbed in lipid tissues such as those of fish, and possibly end up in higher vertebrates when ingested [13]. The pesticides also have varying effects to non-target organisms [14].

Biochar is formed from pyrolysis of biomass in an anaerobic environment in the temperature range of 200–700 ℃ [15]. A wide range of biomasses with different physical and chemical properties have been successfully used to prepare biochar to meet diverse needs [16]. Some of the notably exploited biochar needs include soil amelioration, carbon sequestration and more recently water purification [17, 18]. Biochar has also been used to absorb moisture in compost bins or vermiculture as well as in reduction of bad odors in litter and livestock beddings [18]. Biochar has also been found to serve as a sink for carbon sequestration [18].

Cow-dung in Kenya is a relatively "under-exploited" biomass resource. In the pastoral communities such as in Narok County, cow dung is abundant due to the pastoral activity of its natives [19]. This material has the potential to be utilized for preparation of biochar adsorbents for removal of PAHs and pesticide residues in waste waters. This is because biochar has an excellent combination of physical properties suitable for numerous functions [20]. They include: presence of a porous structure, charged surface, and surface functional groups (such as carboxyl, hydroxyl, phenolic hydroxyl, and carbonyl groups) [20, 21]. Nanoparticle preparation and surface modification studies have also been conducted to enhance the functionalities of carbon [22, 23]. These properties make biochar a suitable candidate for water purification which is a challenge in Narok and Bomet counties and was thus the goal of this study.

In this study, we explore the suitability and efficacy of biochar from locally available cow dung biomass in preparation of water filters. This is in search of locally available filters aimed at eradicating the increasing pesticide residues and PAHs from waters in Narok and Bomet counties, Kenya. The study further delved into various adsorption parameters and models seeking to optimize the adsorption conditions for efficient removal of PAHs and pesticide residues in water using cow dung biochar (CDB).

2 Materials and Methods

Cow dung biomass materials were collected from Narok County, Kenya, specifically cow dung, was obtained from pastoral fields in in the outskirts of Narok town. At least 10 kg dry mass was purposively sampled. The samples were stored in a cooler box and transported to the lab for analysis. Air drying under ambient conditions was performed to reduce moisture of the samples. The samples were then pretreated manually by removing debris, first by hand then using a handheld magnet to removed undesired metallic particles. The biomass was then crushed using a shredding machine (XRido, DZ-600, China) and sieved to a homogenous particle size of 10–15 mm diameter.

2.1 Biochar Pyrolysis

Pyrolysis of the biomass material was done via low-temperature pyrolysis. Biomass of 5.0 kg batches based on the capacity of the carbonizer were fed into the carbonizer hopper and compacted to reduce air-pockets. The carbonizing unit hopper has a combustion diameter of 1.0 m, height 2.0 m, excluding dome height (0.7 m). It has five controlled air perforations (20.0 mm internal diameter) to control the oxidation process with an enclosed chimney system (height 0.3 m by 150.0 mm internal diameter) as indicated in Fig. 1.

Controlled pyrolysis took place by closely maintaing the pyrolysis time to 25–35 min for each batch at 300–350 ℃

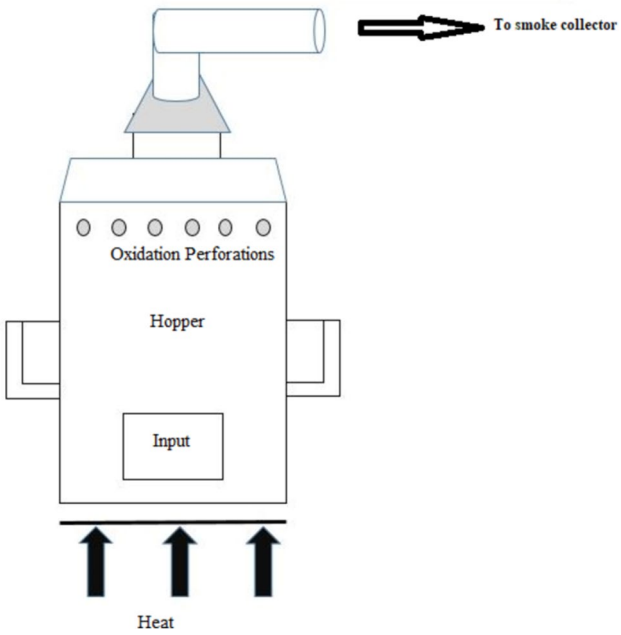

Fig. 1 A picture of the biomass carbonizing unit used to prepare biochar

monitored using a pyrometer (Raytek PM, Model RAY-RPM30L2G, power—9V DC/45mA, USA). This temperature range was chosen to maximize yields while retaining carbon surface sorption properties. Biochar from the carbonizing unit was spread out on a cooler unit – made from enclosed concrete to maximize aeration and heat conduction. The biochar residues were left to cool overnight. The residues were then ground to fine powder which was sieved using a 0.90 µm sieve.

2.2 Biochar Characterization

2.3 Functional Group Analysis

The presence of functional groups in the biochars were investigated using FTIR spectroscopy (Nicolet iS50 FTIR, Thermo, USA). The FTIR spectra of the samples were recorded in the transmittance mode in the range of 4000–500 cm^{-1}.

2.3.1 Surface Morphology

Field Emission Scanning Electron Microscopy (FE-SEM, Joel, Japan) was used to assess the morphological appearance of CDB samples at the Northwest University, South Africa. The images were captured at an operating voltage of 5 kV and a Robinson backscatter detector. Prior to imaging, the samples were coated using the gold sputtering method for 20 s under high vacuum environment to prevent charging.

2.3.2 Elemental analysis

Electron dispersive spectrometry (EDS) was used for identification of the elements present using the FE-SEM. The results were then compared with those obtained by Inductively Coupled Plasma—Optical Emission Spectrometer (ICP-OES); done at Kericho Tea Research Foundation laboratory, Kenya following the method by Pizzanelli et al. [24]. Ionization was conducted by sequential acid digestion of 150 mg of the samples with nitric acid (> 69%) and hydrogen peroxide (analytical grade, > 30%), followed by 2 mL HF (analytical grade, 40%) as per Reza et al., [25]. Boric acid (1.74 g, 98%, solid) and double-distilled water were then added to the 50 mL final volume in a volumetric flask. These measurements were carried out with an Optima 8000 ICP-OES (Perkin Elmer, USA) operating at 1500 W and equipped with an autosampler (Perkin Elmer, S10) and a cyclonic chamber. The different elements were analyzed at varying wavelengths of maximum absorption as per Beer-Lambert Law. The elements present were then determined by comparison with calibration curves obtained using commercial standard solutions.

For X-ray Fluorescence, the samples were sent to Mines and Geology Laboratories and Kenya Revenue Authority (KRA) Laboratories, Nairobi, Kenya. The analyses were done following the method by Jones et al., [26]. Samples were scanned using an X-ray Fluorimeter using the X2B beam. A 1340 × 1300 pixels CCD camera with a pixel size of 4 µm was used to acquire radiographs of the sample using a CsI area X-ray detector. The X-ray energy used for the work was 12.987 keV. Metal contents of the materials were also investigated using micro X-ray fluorescence 88 (XRF) techniques. The beam size was 10 µm.

2.3.3 Crystal Properties and Phases

The crystallinity index of the samples was analyzed using a Shimadzu XRD-700 X-ray Diffractometer at the Northwest University, South Africa. The samples in the form of milled powder were placed on steel sample holders and leveled to obtain total and uniform X-ray exposure. The samples were then analyzed at room temperature (25 ℃) with a monochromatic CuKα radiation source (λ = 0.1539 nm) in the step-scan mode with a 2θ angle ranging from 10° to 80° with a step of 0.04 and scanning time of 5.0 min.

2.3.4 Thermal Properties

A thermogravimetric analyzer (Netzsch STA DSC/TGA, Germany) was used to analyze the thermal properties of the biochar at Northwest University, South Africa. Approximately 0.011 g of the samples were used. The TGA was connected to an inert nitrogen gas flow and heated at a ramping rate of 10 °C/min from 30 to 1000 °C and the weight lost with temperature change was monitored. A sample purge flow using 99.9999% argon gas of 0.0–100 ml/min was used. Differential Scanning Calorimetry (DSC) and Differential Thermal Analysis (DTA) parameters from the TGA analyzer were used to obtain the heat flows of the biochar samples.

2.4 Batch Adsorption Experiments

The batch adsorption studies were conducted at a room temperature (22.5 ± 2 ℃) by agitated measured quantities (2.00 g) of the adsorbents in 100 ml of the prepared standard pollutant solutions comprising of PAHs (naphthalene, phenanthrene and anthracene) and pesticides (α-cypermethrin, λ-cyhalothrin and tebuconazole) all at 1.0 ppb initial sorbate concentration (Co). The standard reaction time adopted for the measurements was 30 min. The agitations were conducted in an orbital shaker at 150 rpm with the required adsorbate parameters including adsorbate pH, reaction temperature, adsorbent dosage, contact time and initial concentration of the adsorbate solutions.

After the adsorption process, the adsorbents were filtered out using a Whatman filter paper (pore size 0.45 µm). The percentage of adsorbate removal was calculated using Eq. 1;

$$\%Removal = 100x\frac{Co - Ce}{Co} \tag{1}$$

Co is the initial adsorbate concentration and Ce is the final equilibrium adsorbate concentration (mg/L). Co and Ce were analyzed via gas chromatography (GC—Perkin Elmer, Clarus 680, UK) hyphenated to mass spectrometry (MS—Perkin Elmer, Clarus 8T) for PAHs and GC—time of flight mass spectrometry (GC-ToFMS, QP 2010SE series, Shimadzu, Japan) for pesticide solutions respectively.

The adsorption capacity, Qe was calculated using Eq. (2);

$$Qe = \frac{(Co - Ce)V}{W} \tag{2}$$

where V is the adsorptive volume of the solution in L, w is the amount of adsorbent used in g, and Qe is the removal efficiency of adsorbent in mg/g.

2.5 Isotherm Models

The optimum adsorption parameters were evaluated and further studied using different adsorption models, namely the Freundlich (Eq. 3), Langmuir (Eq. 4), Dubinin-Radushkevic (Eq. 5), Langmuir–Freundlich (Eq. 6) and Temkins (Eq. 7) models.

$$qeF = KCe^{1/nF} \tag{3}$$

$$qeL = \frac{qmK\mathrm{Ce}}{1 + KCe} \tag{4}$$

$$lnqe = -\beta\left(\varepsilon^2\right) + Lnqm \tag{5}$$

$$qeLF = \frac{qm(KCe)^{nLF}}{1 + (KCe)^{nLF}} \tag{6}$$

$$qe = \frac{RT}{b}(LnA) + \frac{RT}{b}(LnCe) \tag{7}$$

where: qm is the maximum adsorption capacity in mg/g, K is the isotherm constant, which refers to the sorption capacity of the material, n is the isotherm constant, ε is the Polanyi constant used for Dubinin-Rudushkevic equation; b is the Temkin constant (J/mol), T is the absolute temperature (K), R is the gas constant (8.314 J/mol K), and A is the Temkin isotherm constant (L/g). b can be obtained from plots of qe vs LnCe whereby the slope of the plot is RT/b and the y-intercept is RT/b LnA.

The Langmuir separation factor, R_L, was used to determine the favorability of the adsorption process and was calculated by Eq. (8);

$$R_L = \frac{1}{1 + K_L Co} \tag{8}$$

where: K_L is Langmuir constant (mg/g) and Co is initial concentration of adsorbate (mg/g), R_L values indicate the adsorption to be unfavorable when $R_L > 1$, linear when $R_L = 1$, favorable when $0 < R_L < 1$, and irreversible when $R_L = 0$.

The Polanyi constant, ε is quite fundamental in determining whether the adsorption takes place via chemisorption or physisorption. ε is calculated by Eq. (9);

$$\varepsilon = \frac{1}{\sqrt{2\beta}} \tag{9}$$

where ε is the Polanyi constant and β is a constant related to adsorption energy. $\varepsilon < 8.0$ kJ/mol implies a physisorption reaction while $8 < \varepsilon < 16$ kJ/mol implies an ion-exchange and this process is dual (both chemisorption and physisorption). Above 16 kJ/mol, the reaction is chemisorption in nature.

2.6 Kinetic Studies

Several models were used to study the kinetics of the biochar adsorption including, the Lagergren model i.e. pseudo-first-order, PFO (Eq. 10), pseudo-second-order, PSO (Eq. 11), Elovich and Avrami (Eqs. 12 and 13) and fractional power model, FPM (Eq. 14) as described by Puszkarewicz and Kaleta [27]. The differential forms of the models are illustrated below:

$$\frac{dq(t)}{d(t)} = k1(qe - q(t)) \tag{10}$$

$$\frac{dq(t)}{d(t)} = k2(qe - q(t))^2 \tag{11}$$

where t is the time, q the amount of adsorbate bound by the adsorbent (this amount may depend on time), qe corresponds to the value of q in equilibrium, i.e., $q\ (t \to \infty) = qe$, k_1 and k_2 are constants. The kinetics of lead adsorption by the biochar were described by the Elovich (Eq. 12):

$$qe = \frac{1}{\beta}Ln(\alpha\beta) + \frac{1}{\beta}Ln(t) \tag{12}$$

where qt is the quantity of adsorbate adsorbed at time t (mg/g), α (0.035 mg/g/s) is a constant related to chemisorption rate and β (mg/g) is a constant which depicts the extent of surface coverage. The two constants (α and β) can be calculated from the intercept and slope of the plot of qt

versus Lnt respectively. The time-dependent model related to adsorption mechanism is given by the Avrami equation as illustrated in Eq. (13);

$$Ln[-Ln(1-\alpha)] = nAvKAv + nAvLn(t) \quad (13)$$

where KAv is the Avrami constant and nAv is the Avrami model exponent of time related to the change in mechanism of adsorption. KAv and nAv can be obtained from the intercept and slope of the plot of $\ln[-\ln(1-\alpha)]$ against Lnt. The Fractional Power model was also used to describe the rate of adsorption of the pollutants on the adsorbent surface as illustrated in Eq. (14):

$$Lnqt = LnK + vLnt \quad (14)$$

where K and v are constants and v should be less than unity. The sorption rate at is defined as Kv. Log K and v are the intercept and slope of the plot of log q_t against log t respectively thus antilog of intercept gives the value of constant K. v is also a constant that is usually less than unity if adsorption kinetic data fits well into power function model. Qt is the quantity of adsorbate adsorbed at time, t.

2.7 Intra-Particle Diffusion Model

Intra-particle diffusion model was studied using the Weber and Morris model according to Wang and Guo [28] method as indicated in Eq. (15);

$$qt = Kdiff t^{1/2} + C \quad (15)$$

where qt (mg/g) is the amount of pollutants adsorbed at time, t and K_{diff} (mg/g/min$^{-1/2}$) is the rate constant for intra-particle diffusion. The thickness of the boundary layer can also be obtained from the value of C, whereby a large intercept suggests large boundary layer effects. A plot of qt versus $t^{1/2}$ can give a linear indication that intra-particle diffusion is involved in the adsorption process or two or more steps govern the adsorption process.

2.8 Thermodynamics Effects

The thermodynamics effect on adsorption were studied to determine effect of spontaneity and the nature of adsorbate-adsorbent interactions (ΔG°, ΔH° and ΔS°) using Eqs. (16 and 17);

$$LnKo = \frac{\Delta S^\circ}{R} + \frac{\Delta H^\circ}{RT} \quad (16)$$

$$\Delta G^\circ = -RTLnKo \quad (17)$$

where T is the temperature in Kelvin, R is the gas constant and Ko is the adsorption–desorption coefficient and can be obtained from Qe/Ce. A plot of Ln Ko versus 1/T should give a linear plot and ΔH° and ΔS° can be calculated from the slope and intercept respectively.

2.9 Regeneration Studies

Regeneration studies were conducted following isothermal and chemical desorption of the sorbates from the CDB adsorbents according to the method published by Rojas et al. [29]. After the adsorption assays, the adsorbents impregnated with sorbates were centrifuged and the supernatant decanted out. The adsorbents were then soaked in 50.0 ml of 0.01 M $CaCl_2$ solution for two hours with constant agitation at 150 rpm in room temperature conditions. The adsorbents were then washed with excess distilled water three times and left to air-dry for 48 h before re-adsorption. Adsorption capacities for the regenerated adsorbents were evaluated as illustrated in Eqs. 1 and 2.

2.10 Statistical Analysis

Statistical analysis was performed using Origin (Version 2018), Microsoft Excel (version 2016) and Graphpad Prism 9.5.0 (730) for Windows (Prism, USA). Data from analyses conducted was reported as mean ± standard deviation. Correlations were considered to be statistically significant at a 95% confidence interval ($P < 0.05$).

3 Results and Discussion

3.1 Morphological, Crystallinity and Thermal Analyses

The CDB FT-IR spectrum (Fig. 2a) indicated several peaks with potential for adsorbing pollutants at the adsorbent surface. [30].Weak haloalkane stretching bends were observed at 540 cm^{-1} [31]. There were broad symmetric C-O stretches at 1060 cm^{-1} illustrating presence of carbonyl groups associated with carboxylic groups and anhydrides. The sample also indicated a strong C-O stretching aliphatic ether peak at 1190 cm^{-1}. The CDB had a stretching sulfone peak at 1326 cm^{-1}. The sample also had a broad carboxylic –OH stretch peak at 3670 cm^{-1} significant for formation of bands during adsorption of water contaminants [31].

The SEM micrographs of the biochar samples before and after pyrolysis (Fig. 2b, c, d). The micrograph of the raw cow dung indicated spread out particles of different shapes and forms. The difference in brightness of the pyrolyzed micrographs could be clearly observed which could be related to presence of different phases as seen in Fig. 2d [32]. From the micrographs, it is expected that more physisorption would occur, since there were numerous overlapping particles that would lead to adsorption [33]. Feng et al. [34]. observed

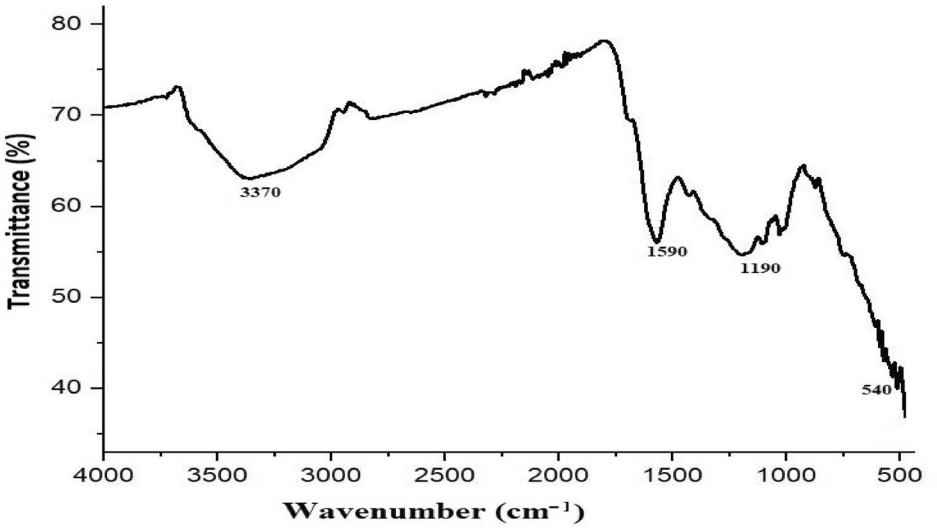

(a)

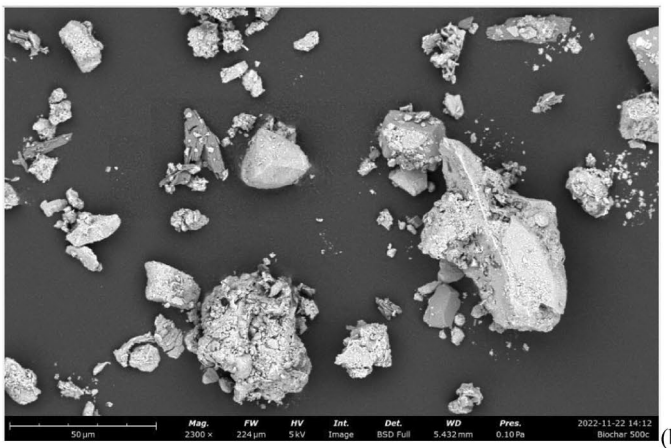

(b)

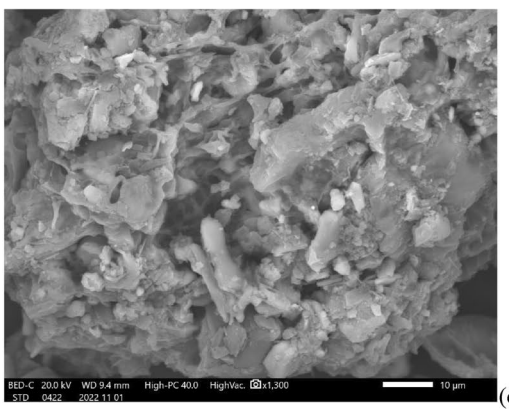

(c)

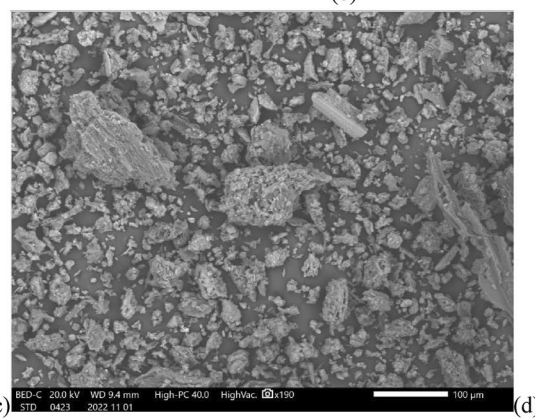

(d)

Fig. 2 FT-IR spectrum (**a**), SEM micrographs before pyrolysis (**b**) and after pyrolysis at 10 µm (**c**) and 100 µm (**d**), XRD diffractogram (**e**) and the TGA and DTG spectra (**f**) of CDB biochar

similar micrographs attributing the 'pockets' causing microbial adhesion.

The XRD spectrum of the biochar (Fig. 2d) exhibited four predominant peaks at different diffraction wavelengths arising from the change in biochar moieties with pyrolysis during preparation [35, 36]. The samples had an amorphous phase characterized by a broad peak between 10 – 25° assigned an XRD plane index of C(101) due to presence of amorphous char combined with hemicellulose and lignin transiting towards biochar in an aromatic polycondensation process [20]. The peak at 17° was attributed to cellulose in CDB [37]. The peak illustrated a plane of graphite structure

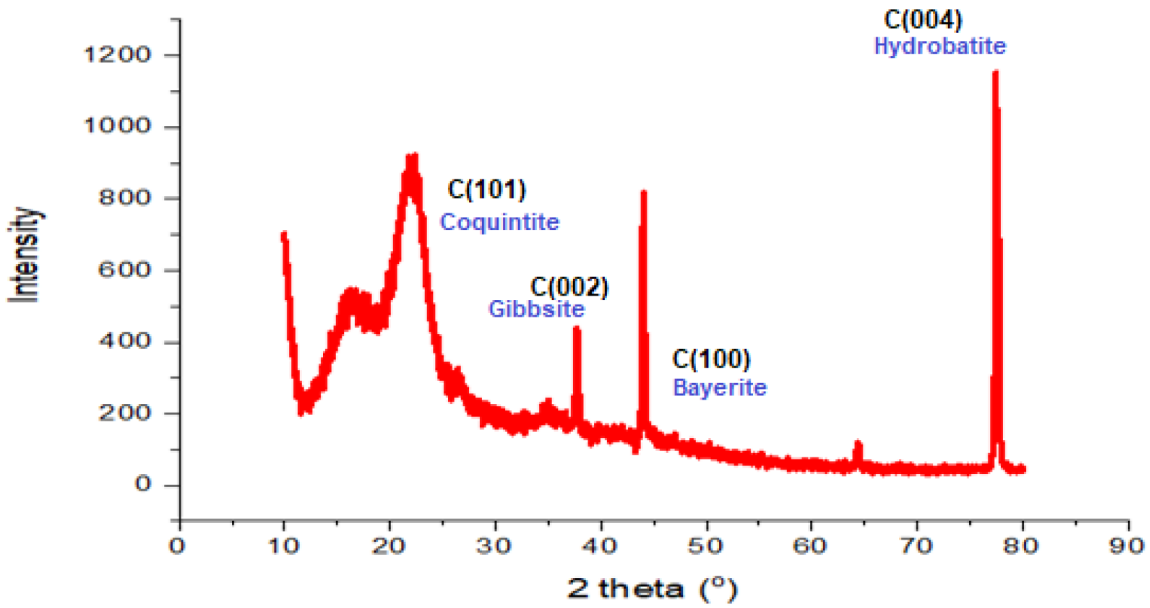

(e)

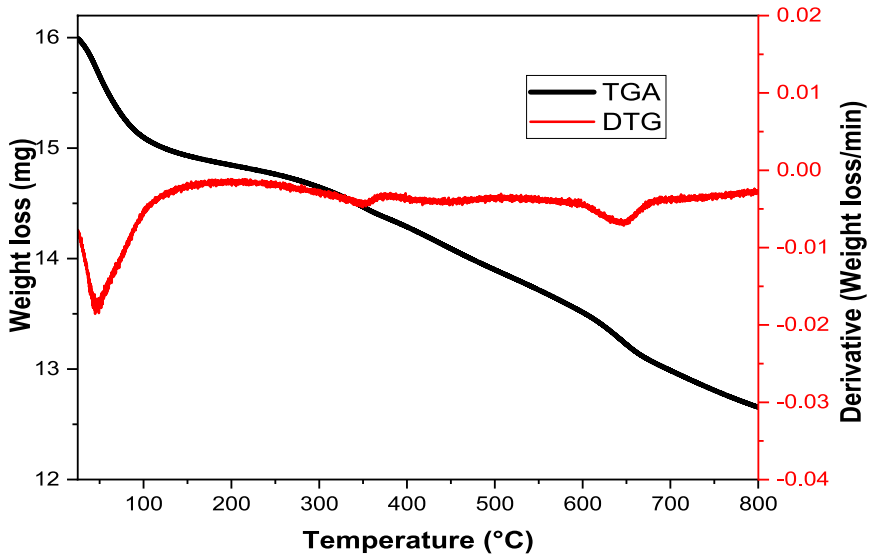

(f)

Fig. 2 (continued)

indicating classic local-order structures of carbon material [37]. At a diffraction wavelength of 38.5°, a transition char phase was observed arising from both organic and inorganic moieties in the biochar samples rising from crystallization of labile organic molecules during pyrolysis [20, 35, 38]. The transition char phase peak in CDB was relatively more intense due to presence of more carbon-ratio in the precursor biomass [39]. The composite char phase peaks at the diffraction wavelength of 44.5° resulted from pyrogenic amorphous carbon formation leading to a composite phase with poorly-ordered graphene stacks [20, 40]. Turbostratic char phase peaks were observed in both biochar samples at a diffraction wavelength of 78.0°. The phase comprises of crystallites of disordered graphite formed from condensation and reordering of carbon atoms during pyrolysis [20, 41]. In general, CDB was found to have irregular peaks (due to presence of inorganic salts) with relatively less intense and broad peaks illustrating amorphousness.

The DTG thermograms of the biochar samples portrayed CDB as being quite thermally stable (Fig. 2e). The dehydration rate was reduced by the low C/H/O ratio nature of CDB matter and presence of inorganic compounds [42]. The net

decrease in the weight of the CDB biochar was relatively low indicating high recalcitrance and thermal stability of CDB [43]. According to Al-Harby et al. [44], the relatively high enthalpy shifts observed for CDB illustrate potential to withstand chemisorption (characterized with high enthalpy changes) when used as adsorbent. These biochar enthalpy shifts were however lower than those obtained for biochar from coconut shell activated carbon/polyethylene glycol (90.2 J/g) [45], almond shells biochar/polyethylene glycol (82.73 J/g [46] and potato activated carbon/polyethylene glycol (91.80 J/g) [47].

The DTG analysis of the biochar samples is illustrated in Fig. 2e. The CDB sample had a relatively stable differential weight loss owing to presence of both non-labile and inorganic matter in this sample. The DTG peak features exhibited four different phases characterized by different chemical reactions leading to weight changes in regards to the original mass of the CDB. The region between 1 and 200 °C was characterized by a sharp dip that rekindled the curve and was followed by slow gradual weight loss. This weight loss is attributed to evaporation of moisture in the sample [37]. The region 200 – 310 °C was also occasioned by a relatively slow weight loss with a slight dip close to 310 °C due to loss of organic matter in CDB. The region between 310 and 450 °C is occasioned by pyrolysis of cellulose, hemicellulose and starch molecules and equally experienced negligible weight losses [48]. Between 450 and 800 °C, carbonization of the CDB took place occasioned by lignin degradation. The peak profile for CDB in this region was equally slow including at 500 °C expected to have charcoal devolatilization [49]. The slow weight loss of CDB was attributed to several phases and inorganic moieties that cause heat recalcitrance [50]. This high temperature recalcitrance property makes CDB a suitable material for extreme temperature water filters.

3.2 Elemental and Oxide Composition Analysis

The carbon:hydrogen:oxygen (C/H/O) content in the CDB biochar was found to be 86.5% as indicated in Table 1. CDB also contained several trace metals such as calcium, potassium, aluminium and iron as well as some of their oxides (Table 2) attributed to the diversity in composition of cow dung arising from different biomass feedstock ingestion [51, 52]. There are also more labile organic matters in cow dung that are easily lost during pyrolysis before formation of recalcitrant compounds [53].

The ICP-OES findings (Table 3) resonated with the EDS findings as far as the composition of CDB biochar were concerned. From the findings, at least 7.72% of the CDB composition was not C/H/O. C/H/O ratios are prone to dehydration process during biochar formation [54] as well as decarboxylation arising from increased cow dung condensation [55]. High carbon content in the starting material is a crucial parameter for the formation of particles with high specific surface area and porosity [37, 56]. There was 0.49% of phosphorus in CDB biochar contributed by presence of proteineous matter in cow dung [57]. This is also critical in regulating high levels of alkalinity as would be formed by the numerous metal alkalis in aqueous media [58].

There were seven detected elements in CDB (Table 3) arising from different raw material composition of CDB. Sulfur, aluminium and tin were all detected in minute concentrations while at least 1.56% of CDB comprised of Fe essential for highly selective adsorption of organic pollutants in water [59]. This arises from the high reactivity of iron

Table 1 The elemental composition of CDB samples by EDS analysis

Element	Mass (%)	Atom (%)
C	51.48 ± 0.18	62.06 ± 0.22
O	35.02 ± 0.33	31.68 ± 0.29
Mg	0.29 ± 0.02	0.17 ± 0.01
Al	1.14 ± 0.03	0.61 ± 0.02
Si	7.99 ± 0.08	4.12 ± 0.04
K	0.55 ± 0.03	0.20 ± 0.01
Ca	2.34 ± 0.05	0.85 ± 0.02
Fe	1.19 ± 0.05	0.31 ± 0.01
Total	100.00	100.00

Table 2 The oxide composition of CDB samples by XRF analysis

Compound	Concentration Unit (%)
Al_2O_3	11.0
SiO_2	37.0
SO_3	0.70
K_2O	4.00
CaO	20.4
TiO_2	1.10
MnO	1.00
Fe_2O_3	24.0
Total	100.0

Table 3 ICP-OES results of the biochar samples

Element	CDB (%)
P	0.49
K	1.01
Ca	3.01
Mg	0.43
Mn	0.103
Al	1.11
Fe	1.56
Total	7.713

with organic ligands leading to larger complexes [60, 61]. From the XRF findings (Table 2), silicon (37.0%) wasthe most abundant element present in CDB and is essential in adsorption of large bio-molecules due to its high ability for formation of hydrogen bonds [62]. The relatively abundant concentration of Si in CDB also makes it suitable in passivating other heavy metal pollutants from wastewater during adsorption process [63].

3.3 Batch Adsorption Experiments of PAHs and Pesticide Residues Using the CDB Adsorbent

Temperature increase was found to favor adsorption of the pollutants up to 10 ℃ after which further increase in temperature did not have a significant effect on the adsorption efficiency using the CDB adsorbent. When PAH pollutants were involved, increase in temperature beyond 10 ℃ led to a slight decrease in Qe to 95%. Anthracene indicated lower adsorption trends when both adsorbents were used with a Ce of 80% as indicated in Fig. 3a. Naphthalene adsorption profile was the highest adsorbed illustrating a positive correlation with increasing temperature. Tebuconazole adsorption profile was significantly lower ($P \leq 0.05$) than for the other pesticides in the CDB system with a Qe of 63%. Several studies confirmed adsorption of pesticides as being exothermic and thus having their adsorption profiles decrease over time [64–67]. From Fig. 3a, the optimal adsorption temperature was 10–20 ℃ which is the average temperature of most water systems. This indicates no additional heating or cooling would be necessary for optimal functioning of the adsorbents.

From Fig. 3b, the pollutants exhibited different adsorption profiles against the reaction time. For PAHs, optimum adsorption was achieved after 40 min with a reduction in Qe being observed after 50 min implying possible desorption. This would be attributed to thermal effects and surface microporosity of the adsorbent sites as well as back diffusion [68]. Naphthalene attained Qe at a higher adsorption capacity compared to the phenanthrene and anthracene but this fell sharply after 50 min. The small size of naphthalene makes it more convenient to fit into the adsorbent pores compared to the other larger PAHs [69]. The eventual Qe for anthracene was relatively larger at the end of the reaction (60 min). Different adsorption profiles for naphthalene have been extensively studied as indicated in Table 4, with the present study concurring with most of the findings of the other studies. The present study however reveals attainment of adsorption equilibrium at a faster rate under ambient conditions and a relatively similar adsorption capacity. This indicates CDB has high potential for naphthalene adsorption from water systems.

The adsorption profiles of phenanthrene and anthracene were closely related, possibly due to their similarity in molecular weights and sizes and thus similar affinity to adsorbent pores. Zhou et al. [76] found a close correlation between PAHs number of rings and the adsorption trends. There was adsorption – desorption profiles of the pesticides especially for λ-cyhalothrin and tebuconazole after 30 min and the Qe remained unchanged until the end of the adsorption process. The Ce for tebuconazole was significantly lower throughout the reaction with a Qe of 81% against 95% and 96% for α-cypermethrin and λ-cyhalothrin respectively. These differences could be attributed to variation in octanol–water partition coefficient values for tebuconazole versus λ-cyhalothrin and α-cypermethrin thus leading to different contact times in water and the adsorbent [77]. The release of molecules beyond 25 min exhibited for all the pesticide adsorption profiles indicate that the adsorption takes place via physisorption or dual adsorption method [66]. This type of adsorption enables desorption of pesticide residues on the adsorbent sites as a result of physical agitation during stirring and with changing chemical environment on the adsorbent sites [66, 70].

All the pollutants indicated maximum Qe at a pH range of of 4.0–8.0 with adsorption efficacy decreasing with increased pH levels beyond 8.0. Adsorption levels of between 90 and 95% were recorded at pH 4.0–6.0 for most of the pollutants (Fig. 3c). The adsorption efficiency of tebuconazole was low with the lowest adsorption occurring at pH 10.0. Similarly, for the PAH pollutants, there were enhanced decline in adsorption efficiency for anthracene with increasing pH value compared to naphthalene and phenanthrene. The optimal adsorption values at acidic media were attributed to high number of charged protons (H^+) which would drive the non-polar PAHs out of the solution to the adsorbent.

Effect of sorbate concentration on adsorption varied significantly with the adsorbents (Fig. 3d). The unsteady adsorption profiles exhibited by CDB can be attributed to irregular surface morphology and composition of CDB leading to weaker adsorption with the adsorbents [78]. There were irregular adsorption profiles with relatively higher adsorption profiles at a concentration of 2.0–4.0 ppb for both PAHs and pesticide residues. Similar trends were observed by Srikhaow et al. [79] for adsorption of pesticides using various biochar adsorbents. Further concentration led to a decline in the adsorption profiles with the desorption being attributed to surface-binding competition compounds formed between CDB compounds and the pollutants. The profile of naphthalene was more enhanced compared to the other PAHs due to the increased reactivity of more volatile PAHs in water [80]. Anthracene adsorption was the least and this would be attributed to the microporous nature of the

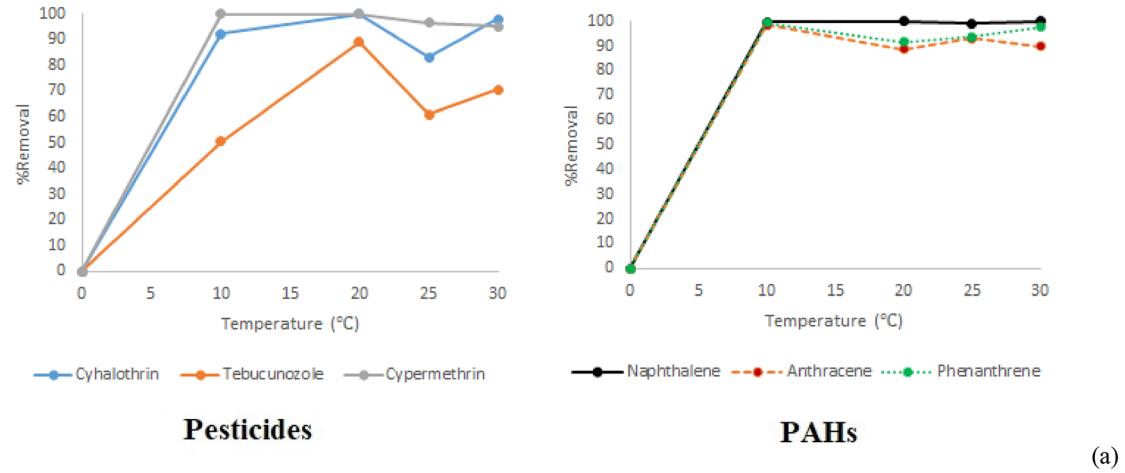

(a)

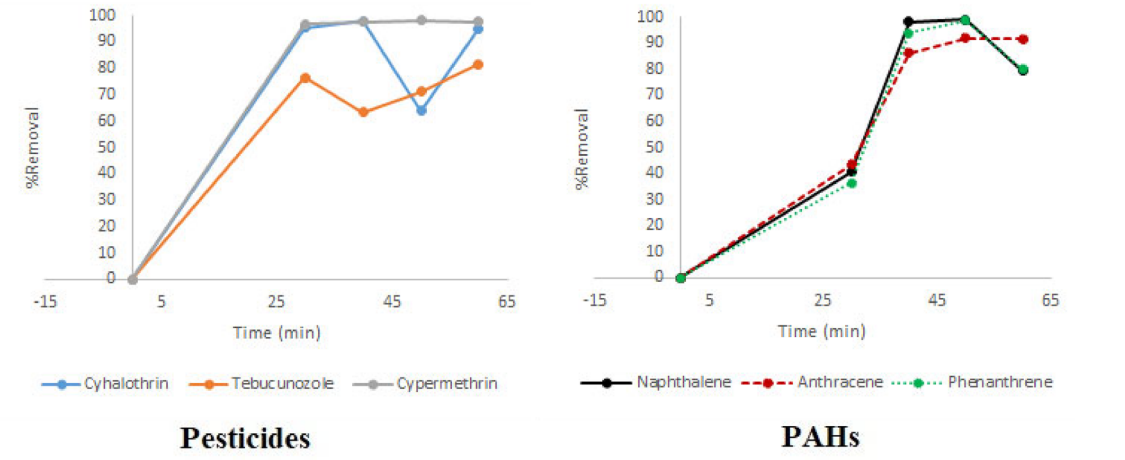

(b)

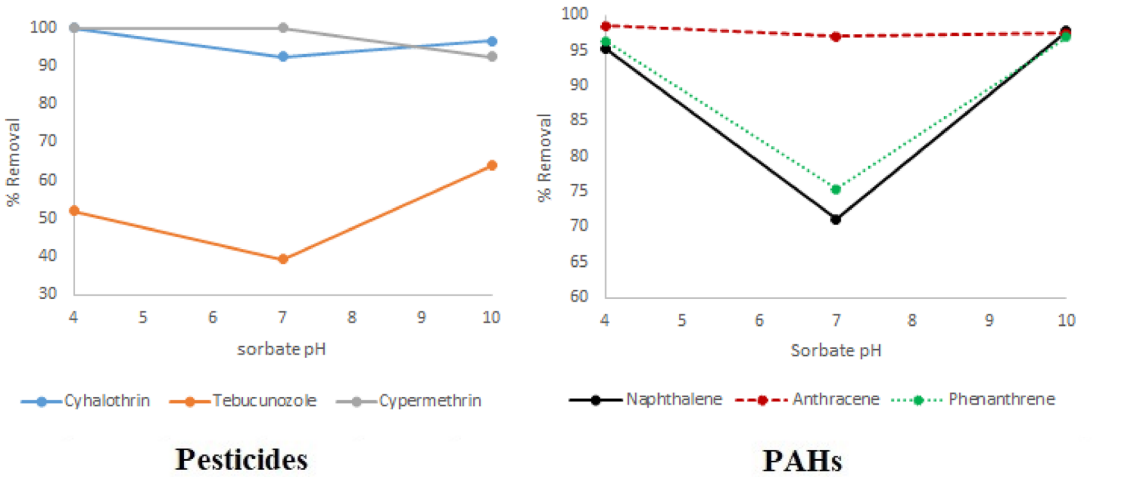

(c)

Fig. 3 Effect of temperature (**a**), reaction time (**b**), sorbate pH (**c**), sorbate concentration (**d**) and sorbent dosage (**e**) on adsorption efficiency. The standard reaction parameters adopted for the varying measurements were: Temperature of 22.5 ± 2 °C, Co of 1.0 ppb, reaction time of 30 min, adsorbent dosage of 2.0 g/100.0 ml adsorbent while pH varied with adsorbates used

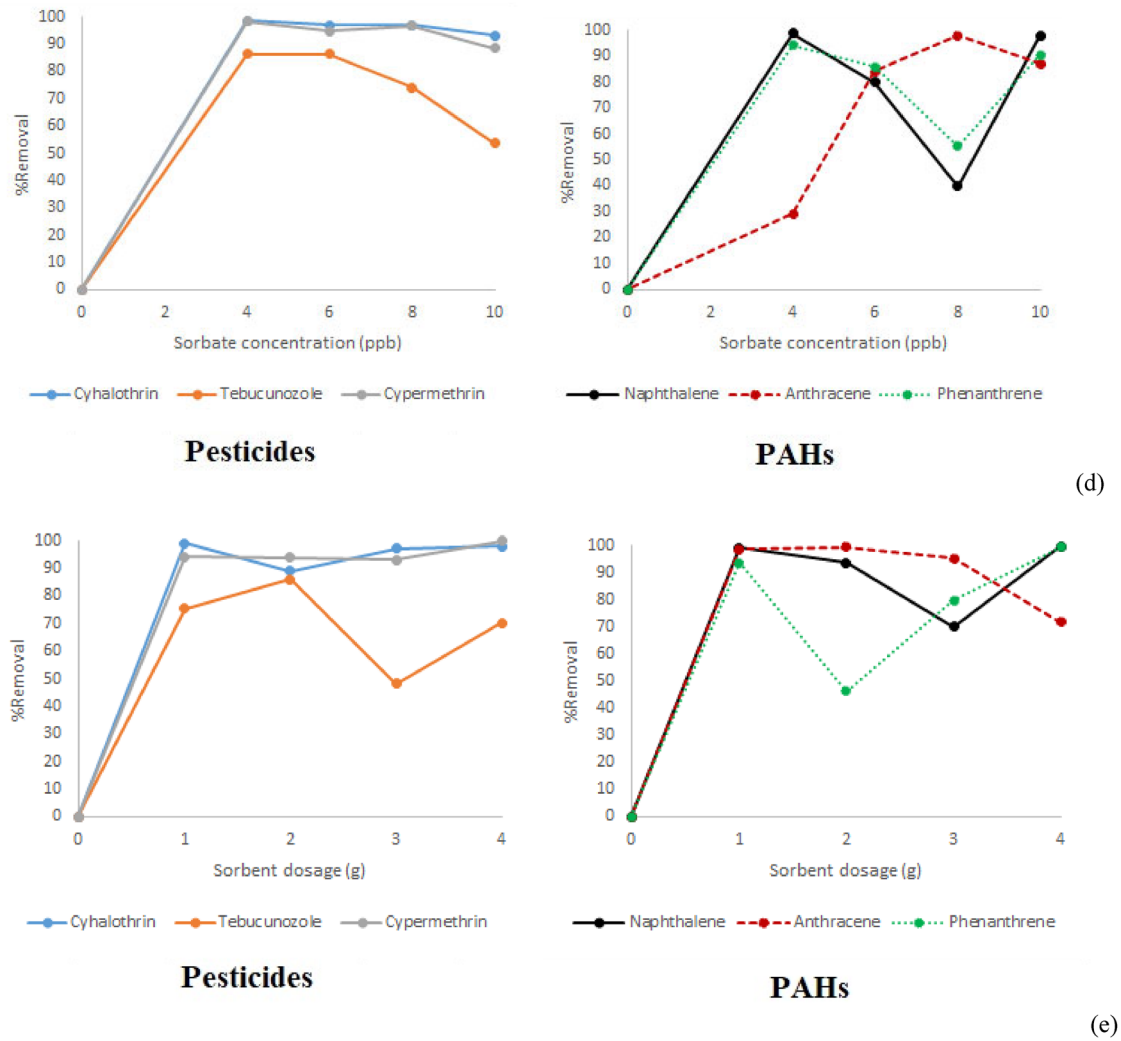

Fig. 3 (continued)

Table 4 A comparative analysis of the contacts time for adsorption of naphthalene with previous studies conducted

Adsorbent	Adsorption Capacity (mg/g)	Optimal Temperature (℃)	Equilibrium Time	References
Activated carbon (commercial)	271.72	20	NA	Iovino et al., [70]
Activated carbon (bean pods)	300	NA	72 h	Cabal et al., [71]
Zeolite	769.23	NA	> 200 min	Chang et al., [72]
Activated carbon (kernel shells)	21.00	28	2 h	Alade et al., [73]
Activated carbon (flamboyant pods)	294.12	28	2 h	Alade et al., [73]
Boehmite nanopowder	200	25	1 h	Abu-Elella et al., [74]
Activated carbon (banana peels)	333.33	20	80 min	Gupta and Gupta, [75]
Cowdung biochar	382 ± 62	10 – 20	40 min	Present study

CDB surface leading to lower adsorption of heavy molecules such as anthracene [81].

The adsorption profiles of the PAHs with varying adsorbent dosage resembled those of the sorbate concentrations (Fig. 3e). There was a reduction of adsorption capacity after 1.0 g of the adsorbent dose for both PAHs and pesticide pollutants. This variation can be explained in terms of the sorbate effective concentration on the adsorbent sites which

is related to the chemical interaction of the sorbates and the adsorbent molecules in water. Apart from tebuconazole, the irregular adsorption profiles experienced while using CDB are attributed to the mesoporous surface of CDB and thus early saturation of the sites.

3.4 Isotherm Models

All the pollutants exhibited negative slopes when subjected to Langmuir and Freundlich adsorption isotherms (Table 5) illustrating that they did not conform to these isotherms. These outcomes were dictated by the nature of the biochar adsorbents used as well as the binding affinity of the pollutants on the surface of the biochar [82]. From Fig. 1, the biochar adsorbent was heterogeneous, rough and non-uniform, thus there was over-stacking of sorbate molecules on the sorbent. The negative slopes evidenced in the Freundlich models also illustrated lack of empirical adsorption conditions as required by this model.

All the Langmuir separation factors, R_L had a value of 1.00 indicating linear though unfavorable adsorption in this model. The non-conformities to the Langmuir model were depicted by the negative slopes and low R^2 values as seen in Table 5. High monolayer saturation capacity was observed for the biochar samples. There were no notable differences in the adsorption capacities amongst the different types of sorbates. The R^2 values for Freundlich and Temkins model were significantly higher than those of Langmuir model ($P \geq 0.05$), clearly indicating that the Langmuir model was not favored. This would be attributed to the heterogeneous and mesoporous nature of the adsorbents and presence of impurities (Table 5), thus leading to interactive effects with neighbors which discourage the Langmuir model [83]. Most of the sorbates also recorded a negative adsorption intensity in the Freundlich model. However, the adsorption capacities when the Freundlich model (1.64–2.75) was used were significantly higher ($P \geq 0.05$) than those of the Langmuir model (-0.13 to -0.73).

Based on the R^2, Temkins model was the most favored adsorption model implying a gradual decline in binding energy with increased adsorption coverage on the CDB sorbent [84]. The adsorption capacities in Temkins model were the highest for all the models tested and ranged between 0.82 and 14.7 mg/g. The diverse range of K_T values indicated variation in the thermal interactions of different pollutants with the adsorbents. The extremely high or low K_T values were due to more number of exposed adsorption sites [85].

The Polanyi constant values, ε and maximum saturation capacity, Qm of the adsorbents as per the Dubinin-Radushkevic isotherms are indicated in Table 6. The biochar samples indicated negative slopes for Dubinin-Radushkevic isotherms. The Qm values were in the range of 3.75–4.48 mg/g attributed to the relatively larger pore volumes in CDB thus creating 'pockets' of adsorption sites. Additionally, the rate of sorbate desorption was found to increase with adsorbent dosage beyond 1.0 g. There was a significant variation in ε with the sorbates due to the morphology of the adsorbent particles lead to more repulsion with incoming sorbate molecules and release higher Gibbs free energy (more entropy). All the sorbates except λ-cyhalothrin exhibited chemisorption or a mixture of the two as the mode of adsorption used. Ambaye et al. [82] illustrates this mode as the most preferred involving use of Van der Waals forces, hydrogen bonding and hydrophobic interactions for biochar while binding with organic pollutants.

Table 6 Dubinin-Radushkevic adsorption isotherm parameters

Sorbate	Qm (mg/g)	ε (KJ/mol)	Nature of Adsorption
λ-cyhalothrin	3.75	7.60	Physiosorption
Tebucunazole	4.18	12.5	Dual
α-cypermethrin	4.24	10.9	Dual
Naphthalene	4.19	12.5	Dual
Anthracene	3.95	8.50	Dual
Phenanthrene	4.48	8.80	Dual

Table 5 Adsorption isotherm parameters for Langmuir, Freundlich and Temkins models for the interaction of CDB and target pesticides and PAHs

Biochar Type	Sorbates	Model												
		Langmuir					Freundlich				Temkins			
		K_L	R_L	Intercept (mg/g)	Slope	R^2	Intercept ($K_{F)}$	Slope (n^{-1})	n	R^2	K_T ($Lmol^{-1}$)	Intercept (mg/g)	Slope	R^2
CDB	λ-cyhalothrin	−0.73	1.00	0.24	−0.33	0.40	1.74	−0.03	−33.3	0.94	0.64	0.82	−1.83	0.95
	Tebucunazole	−0.26	1.00	0.43	−1.66	0.34	2.65	−0.47	−2.13	0.94	0.66	6.26	−14.8	0.98
	α-cypermethrin	−0.37	1.00	0.29	−0.77	0.29	1.76	−0.05	−20.0	0.87	0.45	1.99	−2.52	0.88
	Naphthalene	−0.13	1.00	0.49	−3.89	0.50	2.75	−0.51	−1.96	0.86	0.41	13.7	−15.4	0.92
	Anthracene	−0.17	1.00	0.36	−2.13	0.09	1.64	0.00	1.00	0.49	Too large	14.7	0.11	0.50
	Phenanthrene	−0.37	1.00	0.29	−0.78	0.35	2.18	0.12	8.33	0.88	0.41	8.77	−9.81	0.91

3.5 Kinetic Models

The different sorbates and biochar were found to have varied fittness with the PFO, PSO and Erovich-Akrami kinetic models evaluated. Pesticides adsorption using the biochars were had the best fitted PFO kinetics model with R^2 fitness value of above 0.94 (Fig. 4). This implied that the rate-determining step used in adsorption of the pesticides onto CDB was linear to the initial concentration of these pesticides [28]. The K_f values of the three pesticides were in the order of λ-cyhalothrin (1.02 min^{-1}) > tebuconazole (1.10 min^{-1}) > α-cypermethrin (1.26 min^{-1}). The difference in reaction constants are attributed to different reactivities based on the pesticides functional groups affinity to CDB [82]. Jie et at. [86] found out similar findings in adsorption of cypermethrin onto bacteria consortium immobilized on biochar (K_f value of 0.0422 d^{-1}).

Smaller sorbates are favored by these mode of adsorption thus the pesticides had a larger R^2 fitness value compared to the relatively larger PAHs molecules. Most of the sorbates with good fitness for PSO and undergo both chemisorption and physiosorption as was evidenced from the results presented in Table 6. The PAHs samples indicated positive response to PSO compared to the pesticide samples which all exhibited negative slopes for PSO (Fig. 5). This can be attributed to differences in chemical polarities and thus differing surface reaction by the two groups of compounds [87].

For the PAHs adsorption, both PSO and Erovich-Akrami models indicated a positive slope. However, the slope by Erovich-Akrami had higher R^2 values of above 85% indicating more fitness to this kinetic model compared to the other models (Figs. 5 and 6). The findings illustrate that the rate-determining step of PAHs adsorption onto CDB were governed by energy heterogenity on the CDB surface in

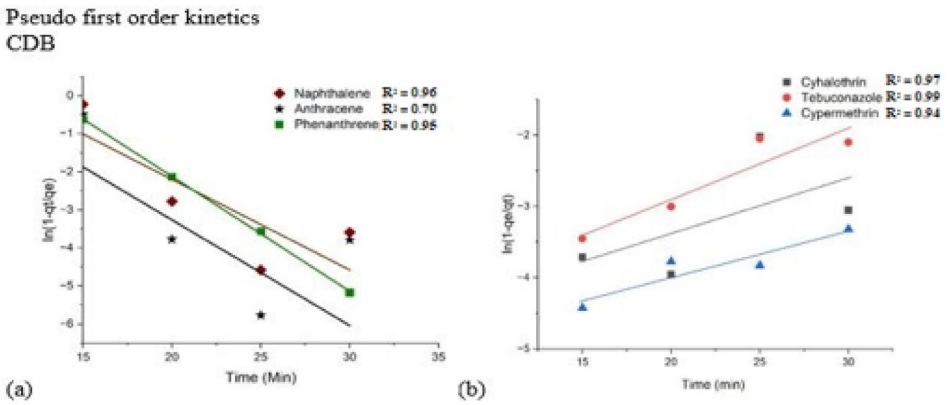

Fig. 4 Pseudo-first order (PFO) kinetic models of the PAHs (**a**) and pesticide (**b**) adsorbates

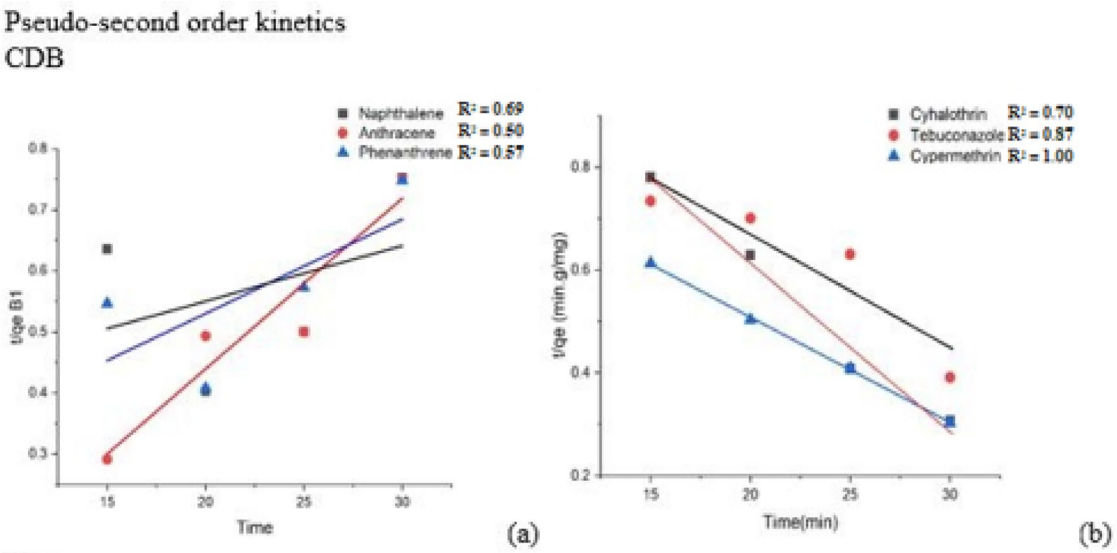

Fig. 5 Pseudo-second order (PSO) kinetic models of the PAHs (**a**) and pesticide (**b**) adsorbates

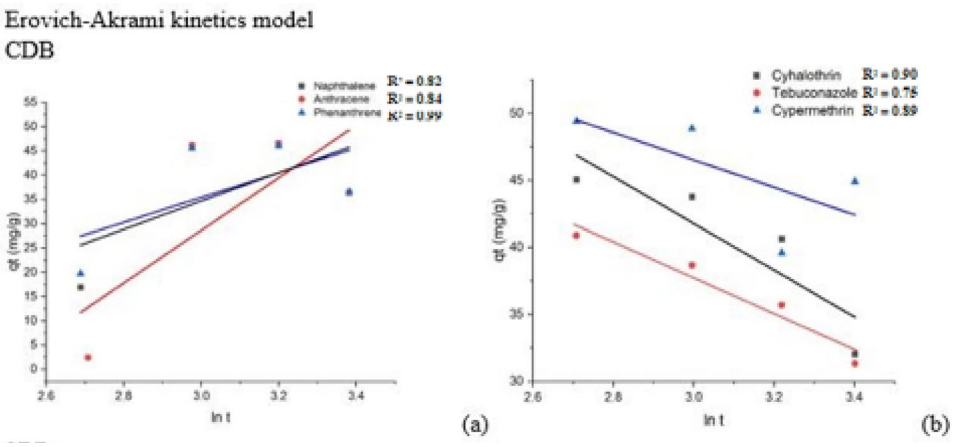

Fig. 6 Avrami-Erovich kinetic models of the PAHs (**a**) and pesticide (**b**) adsorbates

preferance to adsorbate initial concentration or the adsorption capacity of the CDB adsorbent as is the case for PSO models. The desorption constants, β of the three PAHs were in the orders of phenanthrene (0.019 mg/g) < naphthalene (0.034 mg/g) < anthracene (0.039 mg/g). This implies that the extent of surface coverage also increased in this order due to the polarities of these molecules amongst other factors [87]. Wu et al. [88] found similar findings, with R^2 values in the range of 0.84–0.87 during adsorption of single-component and binary naphthalene and phenanthrene on walnut shell based activated carbon. In their study, the desorption constants, β were in the range of 2.48–5.08 mg/g. This indicated that the CDB adsorbent had a longer affinity for PAH sorbates which is a desirable attribute for water filter adsorbents.

From the fractional power model (Fig. 7), it was observed that there was a positive fit to this model for adsorption of PAH ions while that of pesticide ions with sorbents was negative. This difference was attributed to different chemical ion-interactions between the sorbates and their environments leading to adsorption [89]. The y-intercepts of the graphs depict the rates of sorption of these sorbates at any constant time (t = 1) [89]. These rates were in the orders of: naphthalene > phenanthrene > anthracene for the adsorbents due to the reactivities of these PAHs which are in the same order owing to their sizes and mobility [90]. The values of Qt at initial cocentration were all very close to the experimental Qe and the model can thus be used to estimate Qe at minimal concentrations [91]

3.6 Intra-Particle Diffusion Model

The PAHs sorbates indicated a positive fit towards the intra-particle diffusion model unlike the pesticide sorbates for the adsorbents (Fig. 8). The R^2 values (0.54–0.88) were however much lower and depicted a poor Morris-Weber fitness of the PAHs adsorption when using CDB. None of the plots passed through the origin coordinate of the graphs (0,0) thus indicating that adsorption was not controlled by diffusion process in entirety. Other multiple processes such as sorbate concentration, reaction time and temperature must have been involved in the adsorption processes [92]. The y-intercept values of the PAHs sorbates ranged between 25 and 32 mg/g. The Qt values of both adsorbents were in the order of phenanthrene < naphthalene < anthracene attributed to molecular size and reactivity [90]. The enhanced Qt values

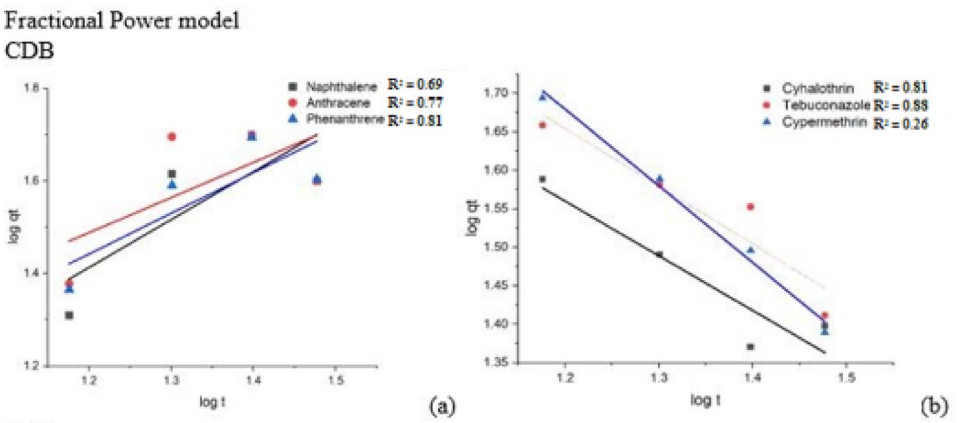

Fig. 7 The Fractional Power Model plots of the PAHs (**a**) and pesticide (**b**) adsorbates

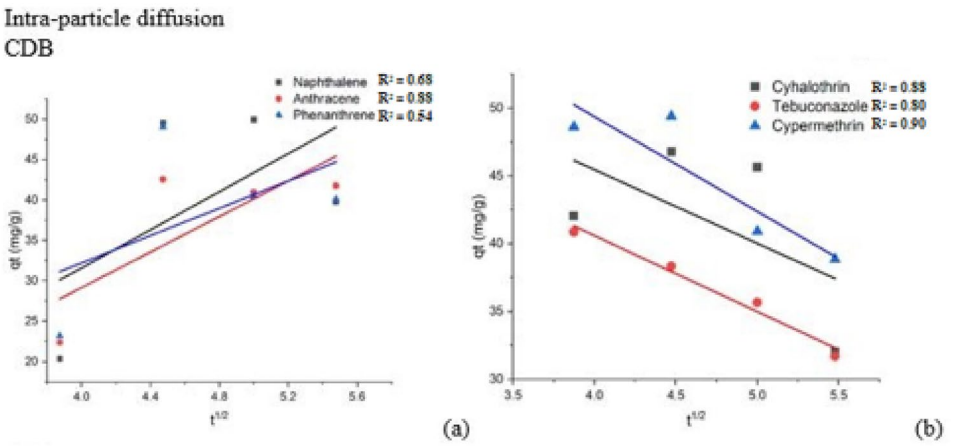

Fig. 8 The Intra-particle difussion model of the PAHs (**a**) and pesticide (**b**) adsorbates

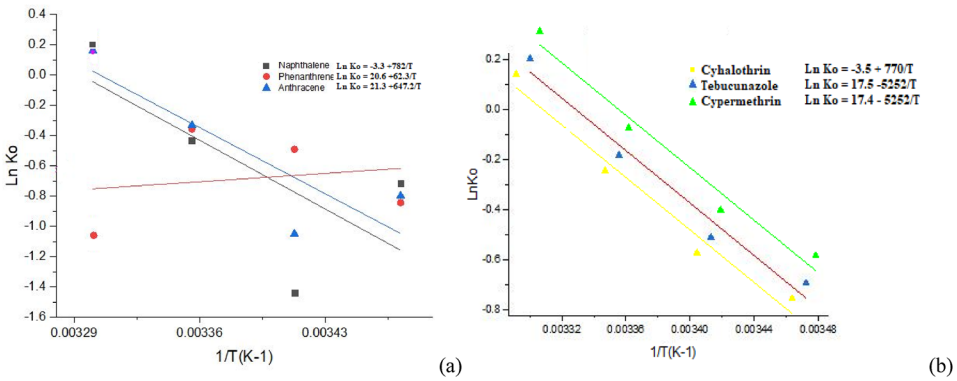

Fig. 9 Van't Hoff plots of the the PAHs (**a**) and pesticide (**b**) adsorbates

can be linked to rapid boundary layer diffusion of sorbates accross liquid films towards adsorbents [93] which common in microporous adsorbents like CDB. The Qt values of anthracene were lower and possibly due to intra-particle diffusion on the macroporous CDB adsorbent [93]. Adsorption of anthracene using this adsorbent is thus desirable due to their fast adsorption of large amounts of sorbates.

3.7 Thermodynamic Studies

The thermodynamic profiles during adsorption of the sorbates onto CDB adsorbents were evaluated as indicated in the Van't Hoff plots in Fig. 9 and the other thermodynamic parameters in Table 7. From the Van't Hoff plots, pesticides sorbates adsorbing onto CDB had better fits to this model compared to the PAHs ones. This implies that there was a linear increase in adsorption (K_o increase) onto CDB with decrease in temperature. The adsorption processes were thus favored with an exothermic reaction up to saturation point. This implies that CDB has high heat tolerance which would be attributed to its composition (Table 1–3). There were some analogous observations made for naphthalene and anthracene which were favored by the Van't Hoff model. The analogous behavior of phenanthrene to the Van't Hoff model

Table 7 Thermodynamic parameters of the sorption processes at room temperature

Sorbate	Thermodynamics Parameters; T = 298 K			
	K_o	ΔH° (KJ/mol)	ΔS° (KJ/mol/K)	ΔG° (KJ/mol)
λ-cyhalothrin	0.01	770	−29.10	−15,073.28
Tebuconazole	0.88	−5252	145.50	−307.62
α-cypermethrin	0.80	−5252	144.66	−555.38
Naphthalene	0.51	782	−27.44	−1674.44
Phenanthrene	0.74	−6230	171.27	−758.24
Anthracene	4.81	6472	177.09	10,658.04

can be alluded to its azeotrope-like behavior upon exposure to high temperature leading to increased spontaneity [94].

The highest K_o value recorded at 298 K was that of anthracene which was also significantly higher ($P \geq 0.05$) than all the rest and implied substantial adsorption for this sorbate. The enhanced K_o value might be as a result of increased kinetic energy for anthracene molecules leading to more adsorption [95]. On contrary, the lowest K_o value recorded was that of λ-cyhalothrin. At least half of the adsorption processes were endothermic (positive ΔH°) while the rest were exothermic (negative ΔH°). All the sorption

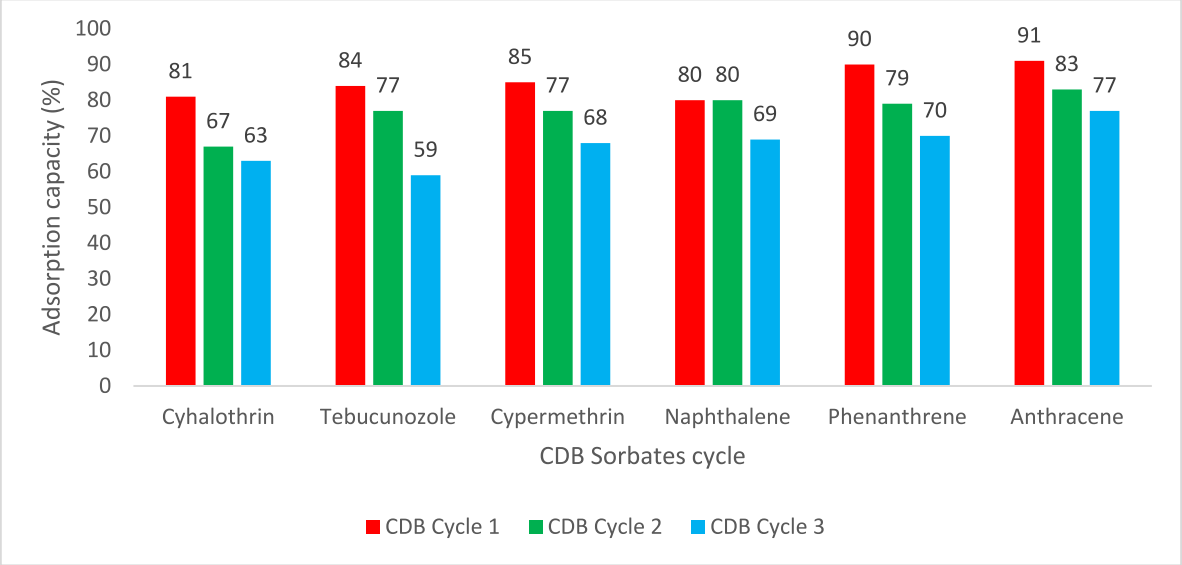

Fig. 10 Regenaration studies of the adsorption processes

processes had ΔH° that were greater than 40 kJ/mol implying they were all chemisorption processes [96]. This would be attributed to the morphology of the sorbents amongst other processes [97]. At least half of the sorbates exhibited positive entropy during the adsorption process at 298 K. Only anthracene had a positive ΔG° value while all the rest had negative ΔG° values indicating they were spontaneous and feasible at this temperature. The findings are quite positive as far as adsorption of PAHs and pesticide residues at room temperature were concerned.

3.8 Regeneration Studies

All the sorbate concentrations decreased with increase in the number of sorption cycles. There were no significant differences in the adsorption capacities of thesorbents and sorbates despite those of the PAHs being slighlty larger than those of the pesticide sorbates ($P \geq 0.05$). There was a significant difference in the first and consequent adsorption cycles for most of the sorbates due to fill-up of adsorbents active sites during the prior adsorption cycles ($P \geq 0.05$). The high levels of adsorption capacities after the third cycle of adsorption (63–80%) as observed in Fig. 10 imply that the adsorbents can be used repeatedly with little decline in efficiency of adsorption [98]. Unlike the findings by Zhou et al. [76], there were no correlation between the regeneration capacities with the number of PAH rings. Isothermal regeneration of biochar adsorbents, as is the case of the current study are preferred for their durability of the adsorbent materials [99].

4 Conclusions

Cow dung biochar (CDB) was successfully prepared by means of a low temperature (300–350 ℃) pyrolysis process in pursuit of determining their adsorption potential for pesticides (tebuconazole, λ-cyhalothrin and α-cypermethrin) and PAHs (naphthalene, phenanthrene and anthracene). CDB exhibited desirable composition, morphological and thermal characteristics that enabled it to adsorb the pesticides and PAHs (78–91% efficiencies). Optimal adsorption took place at sorbate concentration of 4 ppb, 1.5–2.5 g of adsorbent at 10–15 ℃ for a retention time of 30 min and a pH range of 4.0–8.0. Adsorption models were in favor of chemisorption and spontaneous reactions with regeneration capacities if 63–80% for third adsorption cycles.

Supplementary Information The online version contains supplementary material available at https://doi.org/10.1007/s42250-025-01186-3.

Acknowledgements The authors are sincerely grateful to Mr. Evans Suter for his assistance in biochar characterization of FT-IR, XRD, SEM/EDS, BET and TGA/DSC/DTA analysis in Vaal University of Technology and Northwest University, South Africa. We appreciate Mr. Symon Mwangi for his assistance in ICP-OES analysis of the samples in Kericho Tea Research Foundation, Kenya. Ms. Stacy Jemutai of Mines and Geology Lab, Kenya and Mr. Sila Mutinda of Kenya Revenue Authority laboratories were fundamental in XRF analysis samples. Ms. Beatrice Wanjiru of ThermoFischer Labs, Nairobi, Kenya were instrumental in SEM/EDS analysis. Much appreciation to Mr. Maxwell Gitonga, Mr. John Wamumwe, Mr. Denis Kiragu and Mr. Abdallah Marjan for their involvement in preparation of the biochar samples. The authors appreciate Prof. Anthony Gachanja and his Chromatography lab in Jomo Kenyatta University of Agriculture for LC-MS/MS and GC-MS analysis of the adsorbates.

Author Contributions All authors contributed to the study conception and design. Material preparation, data collection and analysis were performed by Bakari Chaka, Aloys Osano, Wesley Omwoyo and Patricia Forbes. The first draft of the manuscript was written by Bakari Chaka and all authors commented on previous versions of the manuscript. All authors read and approved the final manuscript.

Funding The authors declare that no funds, grants, or other support were received during the preparation of this manuscript.

Data Availability All the data used in this work are within the manuscript. Any further data will be provided upon request. "All authors have read, understood, and have complied as applicable with the statement on "Ethical responsibilities of Authors" as found in the Instructions for Authors"

Declarations

Competing Interest The authors have no relevant financial or non-financial interests to disclose.

References

1. Hutton, G., Chase, C.: Water Supply, Sanitation, and Hygiene. In: Mock, C.N., Nugent, R., Kobusingye, O., editors. Injury Prevention and Environmental Health. 3rd edition. Washington (DC): The International Bank for Reconstruction and Development / The World Bank; 2017 Oct 27. Chapter 9. (2017).
2. Pathak VM, Verma VK, Rawat BS, Kaur B, Babu N, Sharma A, Dewali S, Yadav M, Kumari R, Singh S, Mohapatra A, Pandey V, Rana N, Cunill JM (2022) Current status of pesticide effects on environment, human health and it's eco-friendly management as bioremediation: A comprehensive review. Front Microbiol 13:962619
3. Yu-ping L, Wang Y, Ye C, Xie B, Yang H (2017) Sedimentary record of polycyclic aromatic hydrocarbons from the Shuanglong Catchment, Southwest China. J Chem 4976574:10
4. Tarazona JV, Court-Marques D, Tiramani M, Reich H, Pfeil R, Istace F, Crivellente F (2017) Glyphosate toxicity and carcinogenicity: a review of the scientific basis of the European Union assessment and its differences with IARC. Arch Toxicol 91(8):2723–2743
5. Girardin V, Grung M, Meland S (2020) Polycyclic aromatic hydrocarbons: bioaccumulation in dragonfly nymphs (Anisoptera), and determination of alkylated forms in sediment for an improved environmental assessment. Sci Rep 10:10958
6. Patel AB, Shaikh S, Jain KR, Desai C, Madamwar D (2020) Polycyclic aromatic hydrocarbons: sources, toxicity, and remediation approaches. Front Microbiol 11:562813
7. Munyeza CF, Osano AM, Maghanga JK, Forbes PBC (2020) Polycyclic aromatic hydrocarbon gaseous emissions from household cooking devices: a kenyan case study. Environ Toxicol Chem 39:538–547
8. Adeola AO, Nsibande SA, Osano AM, Maghanga JK, Naudé Y, Forbes PBC (2022) Analysis of gaseous polycyclic aromatic hydrocarbon emissions from cooking devices in selected rural and urban kitchens in Bomet and Narok Counties of Kenya. Environ Monit Assess 194(6):435
9. Akkanen J, Tuikka A, Kukkonen JK (2005) Comparative sorption and desorption of benzo[a]pyrene and 3,4,3′,4′-tetrachlorobiphenyl in natural lake water containing dissolved organic matter. Environ Sci Technol 39(19):7529–7534
10. Sakuma, T., Leigh, D., Seto, C., Schreiber, A., Wittrig, R.: Analysis of polycyclic aromatic hydrocarbons (PAH), alkylated derivatives, and photo-degradation products in environmental and food samples using LC-FLD-MS/MS with Q TRAP® Technology. Food Environ AB SCIEX, pp 1–3. (2011).
11. Pérez-Lucas, G., Vela, N., El Aatik, A., & Navarro, S.: Environmental Risk of Groundwater Pollution by Pesticide Leaching through the Soil Profile. IntechOpen. (2019).
12. Aktar W, Sengupta D, Chowodhury A (2009) Impact of pesticides use in agriculture: their benefits and hazards. Interdisciplin Toxicol 2(1):1–12
13. Anaduaka, E. G., Uchendu, N. O., Asomadu, R. O., Ezugwu, A. L., Okeke, E. S., & Chidike Ezeorba, T. P.: Widespread use of toxic agrochemicals and pesticides for agricultural products storage in Africa and developing countries: Possible panacea for ecotoxicology and health implications. Heliyon, 9(4), e15173. (2023).
14. Damalas CA, Eleftherohorinos IG (2011) Pesticide exposure, safety issues, and risk assessment indicators. Int J Environ Res Public Health 8(5):1402–1419
15. Kambo H, Dutta A (2015) A comparative review of biochar and hydrochar in terms of production, physico-chemical properties and applications. Renew Sustain Energy Rev 45:359–378
16. Zhang P, Duan W, Peng H, Pan B, Xing B (2021) Functional biochar and its balanced design. ACS environmental Au 2(2):115–127
17. Xiang L, Harindintwali JD, Wang F, Redmile-Gordon M, Chang SX, Fu Y, He C, Muhoza B, Brahushi F, Bolan N, Jiang X, Ok YS, Rinklebe J, Schaeffer A, Zhu YG, Tiedje JM, Xing B (2022) Integrating biochar, bacteria, and plants for sustainable remediation of soils contaminated with organic pollutants. Environ Sci Technol 56(23):16546–16566
18. Osman AI, Fawzy S, Farghali M, El-Azazy M, Elgarahy AM, Fahim RA, Maksoud MIAA, Ajlan AA, Yousry M, Saleem Y, Rooney DW (2022) Biochar for agronomy, animal farming, anaerobic digestion, composting, water treatment, soil remediation, construction, energy storage, and carbon sequestration: a review. Environ Chem Lett 20(4):2385–2485
19. Iteba JO, Hein T, Singer GA, Masese FO (2021) Livestock as vectors of organic matter and nutrient loading in aquatic ecosystems in African savannas. PLoS ONE 16(9):e0257076
20. Xiao X, Chen B, Chen Z, Zhu L, Schnoor JL (2018) Insight into multiple and multilevel structures of biochars and their potential environmental applications: a critical review. Environ Sci Technol 52(9):5027–5047
21. Liu X, Li G, Chen C, Zhang X, Zhou K, Long X (2022) Banana stem and leaf biochar as an effective adsorbent for cadmium and lead in aqueous solution. Sci Rep 12(1):1584
22. Sanità G, Carrese B, Lamberti A (2020) Nanoparticle surface functionalization: how to improve biocompatibility and cellular internalization. Front Mol Biosci 7:587012
23. Gessner I (2021) Optimizing nanoparticle design and surface modification toward clinical translation. MRS Bull 46(7):643–649
24. Pizzanelli S, Maisano S, Pinzino C, Manariti A, Chiodo V, Pitzalis E, Forte C (2022) The effect of activation on the structure of biochars prepared from wood and from posidonia oceanica: a spectroscopic study. Physchem 2022(2):286–304
25. Reza MT, Lynam JG, Uddin MH, Coronella CJ (2013) Hydrothermal Carbonization: Fate of Inorganics. Biomass Bioenergy 49:86–94
26. Jones K, Ramakrishnan G, Uchimiya M, Orlov A (2015) New Applications of X-ray Tomography in Pyrolysis of Biochar: Biochar Imaging. Energy Fuels 2015:108100
27. Puszkarewicz A, Kaleta J (2020) The efficiency of the removal of naphthalene from aqueous solutions by different adsorbents. Int J Environ Res Public Health 17(16):5969

28. Wang J, Guo X (2020) Adsorption kinetic models: Physical meanings applications and solving methods; A review. J Hazard Mat 390:122156
29. Rojas R, Repetto G, Morillo J, Usero J (2022) Sorption/desorption and kinetics of atrazine, chlorfenvinphos, endosulfan sulfate and trifluralin on agro-industrial and composted organic wastes. Toxics 10(2):85
30. Narayan R, Nayak UY, Raichur AM, Garg S (2018) Mesoporous silica nanoparticles: a comprehensive review on synthesis and recent advances. Pharmaceutics 10(3):118
31. Gale M, Nguyen T, Moreno M, Gilliard-AbdulAziz KL (2021) Physiochemical properties of biochar and activated carbon from biomass residue: influence of process conditions to adsorbent properties. ACS Omega 6(15):10224–10233
32. Zuo W, Zhang W, Liu Y, Han H, Huang C, Jiang W, Mitri H (2022) Pore structure characteristics and adsorption and desorption capacity of coal rock after exposure to clean fracturing fluid. ACS Omega 7(25):21407–21417
33. Di J, Ruan Z, Zhang S, Dong Y, Fu S, Li H, Jiang G (2022) Adsorption behaviors and mechanisms of Cu^{2+}, Zn^{2+} and Pb^{2+} by magnetically modified lignite. Sci Rep 12(1):1394
34. Feng H, Ge Z, Chen W, Wang J, Shen D, Jia Y, Qiao H, Ying X, Zhang X, Wang M (2018) Carbonized cow dung as a high performance and lo cost anode material for bioelectrochemical systems. Front Microbiol 9:2760
35. Cimò G, Kucerik J, Berns AE, Schaumann GE, Alonzo G, Conte P (2014) Effect of heating time and temperature on the chemical characteristics of biochar from poultry manure. J Agric Food Chem 62(8):1912–1918
36. Kumar A, Saini K, Bhaskar T (2020) Hydochar and biochar: Production, physicochemical properties and techno-economic analysis. Biores Technol 310:123442
37. Chen X, Yu G, Chen Y, Tang S, Su Y (2022) Cow dung-based biochar materials prepared via mixed base and its application in the removal of organic pollutants. Int J Mol Sci 23(17):10094
38. Yaashikaa PR, Kumar PS, Varjani S, Saravanan A (2020) A critical review on the biochar production techniques, characterization, stability and applications for circular bioeconomy. Biotechnol Rep 28:e00570
39. Huang W, Chen B (2010) Interaction mechanisms of organic contaminants with burned straw ash charcoal. J Environ Sci 22(10):1586–1594
40. Santos JL, Centeno MA, Odriozola JA (2023) Biochar production from cellulose under reductant atmosphere: influence of the total pyrolysis time. RSC Adv 13(30):21071–21079
41. Cross A, Sohi SP (2011) The priming potential of biochar products in relation to labile carbon contents and soil organic matter status. Soil Biol Biochem 43(10):2127–2134
42. Domingues RR, Trugilho PF, Silva CA, Melo ICNA, Melo LCA, Magriotis ZM, Sánchez-Monedero MA (2017) Properties of biochar derived from wood and high-nutrient biomasses with the aim of agronomic and environmental benefits. PLoS ONE 12(5):e0176884
43. Li S, Chen G (2018) Thermogravimetric, thermochemical, and infrared spectral characterization of feedstocks and biochar derived at different pyrolysis temperatures. Waste management (New York, N.Y.) 78:198–207
44. Al-Harby NF, Albahly EF, Mohamed NA (2021) Kinetics, isotherm and thermodynamic studies for efficient adsorption of Congo red dye from aqueous solution onto novel cyanoguanidine-modified chitosan adsorbent. Polymers 13(24):4446
45. Feng L, Zheng J, Yang H (2011) Preparation and characterization of polyethylene glycol/active carbon composites as shape-stabilized phase change materials. Sol Energy Mater Sol Cells 95:644–650
46. Chen Y, Cui Z, Ding H (2018) Cost-effective biochar produced from agricultural residues and its application for preparation of high-performance form-stable phase change material via simple method. Int J Mole Sci 19:3055
47. Tan B, Huang Z, Yin Z (2016) Preparation and thermal properties of shape-stabilized composite phase change materials based on polyethylene glycol and porous carbon prepared from potato. RSC Adv 6:15821–15830
48. Wang Q, Song H, Pan S, Dong N, Wang X, Sun S (2020) Initial pyrolysis mechanism and product formation of cellulose: An Experimental and Density functional theory (DFT) study. Sci Rep 10(1):3626
49. Fan Y, Lv G, Chen Y, Chang Y, Li Z (2023) Differential effects of cow dung and its biochar on Populus euphratica soil phosphorus effectiveness, bacterial community diversity and functional genes for phosphorus conversion. Front Plant Sci 14:1242469
50. Elkhalifa, S., Parthasarathy, P., Mackey, H.R.: Biochar development from thermal TGA studies of individual food waste vegetables and their blended systems. Biomass Conversion and Biorefinery. (2022).
51. Fasake V, Dashora K (2020) Characterization and morphology of natural dung polymer for potential industrial application as bio-based fillers. Polymers 12(12):3030
52. Behera SS, Ray RC (2020) Bioprospecting of cowdung microflora for sustainable agricultural, biotechnological and environmental applications. Curr Res Microb Sci 2:100018
53. Sarfaraz Q, Silva LSD, Drescher GL (2020) Characterization and carbon mineralization of biochars produced from different animal manures and plant residues. Sci Rep 10:955
54. Batista EMCC, Shultz J, Matos TTS (2018) Effect of surface and porosity of biochar on water holding capacity aiming indirectly at preservation of the Amazon biome. Sci Rep 8:10677
55. Francioso O, Sanchez-Cortes S, Bonora S, Roldán ML, Certini G (2011) Structural characterization of charcoal size-fractions from a burnt *Pinus pinea* forest by FT-IR, Raman and surface-enhanced Raman spectroscopies. J Mol Struct 994:155–162
56. Muigai HH, Bordoloi U, Hussain R, Ravi K, Moholkar VS, Kalita P (2021) A comparative study on synthesis and characterization of biochars derived from lignocellulosic biomass for their candidacy in agronomy and energy applications. Int J Energy Res 45:4765–4781
57. Li G, Li H, Leffelaar PA, Shen J, Zhang F (2014) Characterization of phosphorus in animal manures collected from three (dairy, swine, and broiler) farms in China. PLoS ONE 9(7):e102698
58. Glaser B, Lehr VI (2019) Biochar effects on phosphorus availability in agricultural soils: A meta-analysis. Sci Rep 9:9338
59. Chen F, Wang K, Shao L, Muhammad Y, Wei Y, Gao F, Wang X, Cui X (2019) Synthesis of $Fe2O_3$-modified porous geopolymer microspheres for highly selective adsorption and solidification of F− from waste-water. Compos B Eng 178:107497
60. Briat JF, Curie C, Gaymard F (2007) Iron utilization and metabolism in plants. Curr Opin Plant Biol 10(3):276–282
61. Chobot V, Hadacek F (2010) Iron and its complexation by phenolic cellular metabolites: from oxidative stress to chemical weapons. Plant Signal Behav 5(1):4–8
62. Lewandowski D, Bajerlein D, Schroeder G (2014) Adsorption of hydrogen peroxide on functionalized mesoporous silica surfaces. Struct Chem 25:1505–1512
63. Lin H, Chen T, Yan B, Huang Z, Zhou Y, Huang J, Xiao XA (2020) Functionalized silicate adsorbent and exploration of its adsorption mechanism. Molecules 25(8):1820
64. Aksu Z, Kabasakal E (2005) Adsorption characteristics of 2,4-dichlorophenoxyacetic acid (2,4-D) from aqueous solution on powdered activated carbon. J Environ Sci Health B 40:545–570
65. Fontecha-Camara MA, Lopez-Ramon MV, Lvarez-Merino MA, Moreno-Castilla C (2006) Temperature dependence of herbicide

adsorption from aqueous solutions on activated carbon fiber and cloth. Langmuir 22:9586–9590
66. Pastrana-Martinez LM, Lopez-Ramon MV, Moreno-Castilla C (2009) Adsorption and thermal desorption of the herbicide fluroxypyr on activated carbon fibers and cloth at different pH values. J Coll Interf Sci 331:2–7
67. Daneshvar N, Aber S, Khani A, Khataee AR (2007) Study of imidaclopride removal from aqueous solution by adsorption onto granular activated carbon using an on-line spectrophotometric analysis system. J Hazard Mater 144:47–51
68. Yang X, Li Z, Liu Y, Xing Y, Wei J, Yang B, Zhang C, Yang RT, Tsai CJ (2019) Research progress of gaseous polycyclic aromatic hydrocarbons purification by adsorption. Aerosol Air Qual Res 19:911–924
69. Yang X, Wan Y, Zheng Y, He F, Yu Z, Huang J, Wang H, Ok YS, Jiang Y, Gao B (2019) Surface functional groups of carbon-based adsorbents and their roles in the removal of heavy metals from aqueous solutions: A critical review. Chem Eng J 366:608–621
70. Iovino P, Canzano S, Capasso S, Natale MD, Erto A, Lama A, Musmarra D (2013) Single and competitive adsorption of toluene and naphthalene onto activated carbon. Chem Eng Trans 32(2013):67–72
71. Cabal B, Budinova T, Ania CO, Tsyntsarski B, Parra JB, Petrova B (2009) Adsorption of naphthalene from aqueous solution on activated carbons obtained from bean pods. J Hazard Mater 161:1150–1156
72. Chang CF, Chang CY, Chen KH, Tsai WT, Shie JL, Chen YH (2004) Adsorption of naphthalene on zeolite from aqueous solution. J Coll Interf Sci 277:29–34
73. Alade AO, Amuda OS, Afolabi TJ, Okoya AA (2012) Adsorption of naphthalene onto activated carbons derived from milk bush kernel shell and flamboyant pod. J Environ Chem Ecotoxicol 4:124–132
74. Abu-Elella R, Ossman ME, Abd-Elfatah M, Elgendi A (2013) Kinetic modeling and isotherm study for naphthalene adsorption on boehmite nanopowder. Desalin Water Treat 51:3472–3481
75. Gupta H, Gupta B (2016) Adsorption of polycyclic aromatic hydrocarbons on banana peel activated carbon. Desalin Water Treat 57(20):9498–9509
76. Zhou X, Shi L, Moghaddam TB, Chen M, Wu S, Yuan X (2021) Adsorption mechanism of polycyclic aromatic hydrocarbons using wood waste-derived biochar. J Hazard Mater 425:128003
77. Khawar MI, Mahmood A, Nabi D (2022) Exploring the role of octanol-water partition coefficient and Henry's law constant in predicting the lipid-water partition coefficients of organic chemicals. Sci Rep 12(1):14936
78. Pang Y, Zhao C, Li Y (2022) Cadmium adsorption performance and mechanism from aqueous solution using red mud modified with amorphous MnO_2. Sci Rep 12:4424
79. Srikhaow A, Win EE, Amornsakchai T, Kiatsiriroat T, Kajitvichyanukul P, Smith SM (2023) Biochar derived from pineapple leaf non-fibrous materials and its adsorption capability for pesticides. ACS Omega 8(29):26147–26157
80. Nowakowski M, Rykowska I, Wolski R (2022) Polycyclic Aromatic Hydrocarbons (PAHs) and their Derivatives (O-PAHs, N-PAHs, OH-PAHs): Determination in Suspended Particulate Matter (SPM) – a Review. Environ Proc 9:2
81. Rai PK, Sonne C, Brown RJC, Younis SA, Kim KH (2022) Adsorption of environmental contaminants on micro- and nanoscale plastic polymers and the influence of weathering processes on their adsorptive attributes. J Hazard Mater 427:127903
82. Ambaye TG, Vaccari M, van Hullebusch ED (2021) Mechanisms and adsorption capacities of biochar for the removal of organic and inorganic pollutants from industrial wastewater. Int J Environ Sci Technol 18:3273–3294
83. Hasan IMA, Assaf FH, Tawfik AR (2023) Facile and green synthesis of CuS-activated carbon nanocomposite from Sargassum siliquastrum biomass for fast and efficient removal of eosin yellow dye. Biom Conv Biorefine 14:29873–29899
84. Zand AD, Abyaneh MR (2020) Adsorption of Lead, manganese, and copper onto biochar in landfill leachate: implication of nonlinear regression analysis. Sustain Environ Res 30:18
85. Piccin, J; Dotto, L. and Pinto, A.: Adsorption Isotherms and Thermochemical Data of FD&C Red N° 40 Binding by Chitosan, Brazilian Journal of Chemical Engineering. 28(02), 295–304. (2011).
86. Jie L, Ding Y, Ma L, Gao G, Wang Y (2017) Combination of biochar and immobilized bacteria in cypermethrin-contaminated soil remediation. Int Biodeter Biodegrad 120:15–20
87. Inyinbor A, Adekola F, Olatunji G (2016) Kinetics, isotherms and thermodynamic modeling of liquid phase adsorption of Rhodamine B dye onto Raphia hookerie fruit epicarp. Water Res Indus 15:14–27
88. Wu Z, Sun Z, Liu P, Li Q, Yang R, Yang X (2020) Competitive adsorption of naphthalene and phenanthrene on walnut shell based activated carbon and the verification via theoretical calculation. RSC Adv 10(18):10718
89. Netzahuatl-Muñoz AR, Cristiani-Urbina MC, Cristiani-Urbina E (2015) Chromium Biosorption from Cr(VI) Aqueous Solutions by *Cupressus lusitanica* Bark: Kinetics Equilibrium and Thermodynamic Studies. PLoS ONE 10(9):e0137086
90. Chen W, Yu F, Xu Q, Zhou G, Zhang Q (2020) Recent Progress in High Linearly Fused Polycyclic Conjugated Hydrocarbons (PCHs n > 6) with Well-Defined Structures. Adv Sci 7(12):1903766
91. Gharibzadeh F, Kalantary RR, Esrafili A, Ravanipour M, Azari A (2019) Desorption kinetics and isotherms of phenanthrene from contaminated soil. J Environ Health Sci Eng 17(1):171–181
92. Min P, Xumeng L, Jingjing X, Xiaoming H (2017) Kinetic, equilibrium and thermodynamic studies for phosphate adsorption on aluminum hydroxide modified palygorskite nano-composites. RSC Adv 7(8):4492–4500
93. Simonin JP, Bouté J (2016) Intraparticle diffusion-adsorption model to describe liquid/solid adsorption kinetics. Mexican J Chem Eng 15(1):161–173
94. Rice JW, Fu J, Sandström E, Ditto JC, Suuberg EM (2015) Thermodynamic study of (anthracene + phenanthrene) solid state mixtures. J Chem Thermodyn 90:79–86
95. Yu S, Bo J, Meijun Q (2018) Molecular dynamic simulation of self- and transport diffusion for $CO_2/CH_4/N_2$ in low-rank coal vitrinite. Energy Fuels 32(3):3085–3096
96. Mabuza M, Premlall K, Daramola MO (2022) Modelling and thermodynamic properties of pure CO_2 and flue gas sorption data on South African coals using Langmuir, Freundlich, Temkin, and extended Langmuir isotherm models. Int J Coal Sci Technol 9:45
97. Ahmed A-M, Ali A, Ghazy AH (2019) Adsorption separation of nickel from wastewater by using olive stones. Adv J Chem - Sec A 2(1):79–93
98. Jia L, Cheng P, Yu Y, Chen S, Wang W, He C, Nie H, Wang J, Zhang J, Fan B, Jin Y (2023) Regeneration mechanism of a novel high-performance biochar mercury adsorbent directionally modified by multimetal multilayer loading. J Environ Manage 326:116790
99. Alsawy T, Rashad E, El-Qelish M (2022) A comprehensive review on the chemical regeneration of biochar adsorbent for sustainable wastewater treatment. NPJ Clean Water 5:29